Neurophotonics

Neurophotonics.SPIEDigitalLibrary.org

Differential effects of early postinjury treatment with neuroprotective drugs in a mouse model using diffuse reflectance spectroscopy

Ariel Shochat
David Abookasis

SPIE.

Neurophotonics 2(1), 015001 (Jan–Mar 2015)

Differential effects of early postinjury treatment with neuroprotective drugs in a mouse model using diffuse reflectance spectroscopy

Ariel Shochat and David Abookasis*
Ariel University, Department of Electrical and Electronics Engineering, Ariel 40700, Israel

Abstract. The time required for the arrival of an ambulance crew and administration of first aid is critical to clinical outcome, particularly in the case of head injury victims requiring neuroprotective drugs following a car accident, falls, and assaults. Short response times of the medical team, together with proper treatment, can limit injury severity and even save a life before transportation to the nearest medical center. We present a comparative evaluation of five different neuroprotective drugs frequently used in intensive care and operating units in the early phase following traumatic brain injury (TBI): hypertonic saline (HTS), mannitol, morphine, melatonin, and minocycline. The effectiveness of these drugs in terms of changes in brain tissue morphology (cell organelle size, density, distribution, etc.) and biochemical tissue properties (chromophores' content) was experimentally evaluated through analysis of the spectral reduced scattering and optical absorption coefficient parameters in the near-infrared (NIR) optical range (650 to 1000 nm). Experiments were conducted on anesthetized male mice subjected to a noninvasive closed head weight-drop model of focal TBI ($n = 50$ and $n = 10$ control) and monitored using an NIR diffuse reflectance spectroscopy system utilizing independent source–detector separation and location. After 10 min of baseline measurement, focal TBI was induced and measurements were conducted for 20 min. Subsequently, a neuroprotective drug was administrated and measurements were recorded for another 30 min. This work's major findings are threefold: first, minocycline was found to improve hemodynamic outcome at the earliest time postinjury. Second, HTS decreased brain water content and inhibited the increase in intracranial pressure. Third, the efficacy of neuroprotective drugs can be monitored noninvasively with diffuse reflectance spectroscopy. The demonstrated ability to noninvasively detect cerebral physiological properties following early administration of neuroprotective drugs underlines the need for more extensive investigation of the combined use of clinical drugs in larger-scale preclinical experiments to find the most beneficial drug treatment for brain injury patients. © *2015 Society of Photo-Optical Instrumentation Engineers (SPIE)* [DOI: 10.1117/1.NPh.2.1.015001]

Keywords: neuroprotective drug; focal traumatic brain injury; diffuse reflectance; optical properties; cerebral hemodynamics; scattering.

Paper 14062RR received Sep. 2, 2014; accepted for publication Dec. 31, 2014; published online Jan. 22, 2015.

1 Introduction

Traumatic brain injury (TBI) is a major cause of death and disability worldwide, resulting from the impact of an external force, causing immediate damage and subsequent disruption of brain function. There are two major types of TBI: penetrating (direct impact, such as bullet) and closed head (indirect impact, such as resulting from a car accident) injuries. The latter injury causes two types of brain damage: primary (skull fracture, contusions, hematomas, and nerve damage) and secondary (brain swelling, epilepsy, intracranial infection, raised intracranial pressure, etc.) injury. Common to all head injuries is the excitotoxicity mechanism, caused primarily by excessive glutamate neurotransmission, leading to a cascade of pathophysiological events resulting in tissue damage and associated neuronal cell death. Because the primary injury is considered irreversible, the main focus of clinical intervention is to prevent further neurological decline by reversing or preventing secondary injury.[1–5]

Thus, management of head injury focuses on preventing, detecting, and correcting the secondary brain injury following trauma. Strategies include immediate drug intervention and therapeutic strategies, as well as diagnostics. Specifically, neuromonitoring diagnostic techniques, such as computed axial tomography, magnetic resonance imaging, and positron emission tomography, are extensively used for injury monitoring and evaluation.[6,7] However, these techniques are technically complex and expensive, are not portable, and cannot be used near bedside for continuous, real-time monitoring. Optical methods, on the other hand, can overcome these restrictions as they possess many advantages, such as: (1) relatively inexpensive, (2) portable (bedside monitoring), (3) free from adverse effects of repeated use, (4) easy to maintain, (5) sensitive to several physiological parameters, and (6) offer high spatiotemporal resolution. Intensive investigation in both laboratory and clinical settings over the past four decades has significantly advanced optical platforms for biomedical applications.[8,9] Nonetheless, the detection depth of optical imaging is still limited due to marked light scattering within biological tissue.

Neuroprotection is a principal goal of brain trauma treatment, by preventing and treating complications that frequently result in brain dysfunction. Over the years, a number of neuroprotective agents, which may reduce the extent of secondary brain injuries or prevent their onset, have been identified. A growing

*Address all correspondence to: David Abookasis, E-mail: davida@ariel.ac.il

0091-3286/2015/$25.00 © 2015 SPIE

number of reports have demonstrated the effectiveness of administration of neuroprotective agents to decrease the severity and complication of brain injury.[10,11] In general, neuroprotective drugs include an enormous array of moieties of diverse origins that support the structural-functional integrity of the central nervous system. They also protect against neurodegeneration and neurotoxins. For the reader's knowledge, most anesthetic agents are neuroprotective because of their ability to reduce the cerebral metabolic rate, which has a beneficial impact on the balance between brain energy supply and demand. Anesthetics also increase neuronal tolerance to hypoxic/ischemic injury. Due to drugs' limited passage of the blood–brain barrier (BBB) and their limited half-lives, relatively large doses of neuroprotective agents are usually given via the systemic circulation in order for an effective dose to enter the brain.[12] While some neuroprotective drugs have failed to demonstrate beneficial effects in clinical trials of TBI, other approved agents have shown some clinical success in terms of patients' recovery of function after TBI or stroke.[13–16] Since neuroprotective drugs can be delivered in the field and are considered safe for different types of brain injury, their administration to TBI patients soon after trauma will improve patients' chances of survival and recovery.[17] In this work, we arbitrarily selected five out of hundreds of drugs in common clinical use for treatment of head injury victims, namely hypertonic saline,[18] mannitol,[19] morphine,[20] melatonin,[21] and minocycline.[22] A short description of each is given in the Results section.

In the present study, we assess the effects of the above-mentioned five different neuroprotective drugs following TBI in an animal model. Specifically, anesthetized mice underwent a closed head injury (CHI) paradigm of TBI induced by a weight-drop apparatus. This method is a well-established CHI model shown to trigger a cascade of neurophysiological deficits and cell death.[23,24]

Because of the aforementioned advantage of using optical techniques rather than conventional neuroimaging modalities, multiple optical techniques have been established to detect tissue abnormalities. These include the diffuse reflectance spectroscopy (DRS) system. DRS, also known as near-infrared spectroscopy, is a rapid, noninvasive optical spectroscopic monitoring system that has been successfully applied previously to provide qualitative and quantitative information regarding the biochemical composition (chromophore content) and morphological parameters of biological tissue.[25–29] In its simplest configuration, DRS entails a broadband light source (emitter), detector, and a pair of optical fibers separated by a fixed (or variable) distance for delivery and collection of measurements (optode probe). The measured reflectance is mathematically analyzed to extract the optical properties of the sample under test. It has been shown that the distance between the source and detection points determines the sensitivity of the measured reflectance as a function of the absorption coefficient in the case of large separation distances (>10 mm) and as a function of the scattering coefficient in the case of short separations (<1 mm).[30,31] Therefore, we utilized a modified DRS setup to manipulate properties' sensitivities by employing different source–detector distances and locations, as described below. Since CHI is immediately followed by alterations in the composition and structure of brain tissues,[32,33] and post-trauma medical intervention also induces direct changes in tissue's optical properties, we propose that DRS can aid the diagnosis and monitoring of CHI treatment. Thus, the objectives of the current study were (1) to compare and evaluate the effects of five different commonly used neuroprotective drugs, administrated 20 min after CHI, on pathophysiological changes in the brain and (2) to identify the most effective drug, among the five tested, for injury treatment in this animal model. Overall, our results demonstrate that dynamic response to drug treatment after brain trauma can be successfully investigated with our DRS configuration, which can effectively identify the most efficient drug for CHI treatment. To the best of our knowledge, this is the first comparative evaluation report of neuroprotective drugs' efficacy following CHI by using DRS setup. Our earlier works with different optical platforms showed evidence of morphological and physiological impairments in a mouse model of focal TBI.[34,35] However, the effects of neuroprotective drugs for mitigating brain damage associated with TBI was not investigated previously using DRS. The long-term goal of the present research is to perform extensive investigation of a wide range of clinical drugs to identify the most efficient neuroprotective drug treatment strategy for brain injury patients.

The continuation of this paper is organized as follows. In Sec. 2, we describe the experimental protocol, instrumentation setup, data processing, and provide details of tissue property measurement. Experimental results accompanied with discussion are presented in Sec. 3. Finally, conclusions are included in Sec. 4.

2 Materials and Methods

2.1 *Animal Protocol*

Sixty male mice (ICR, ~12 weeks, ~40 g) were obtained from Harlan Laboratories (Jerusalem, Israel). Each animal was intravenously anesthetized with a cocktail containing ketamine (80 mg/kg), xylazine (20 mg/kg), and saline (NaCl, 0.9%). The depth of anesthesia was ascertained by manually pinching the toes or tail and by monitoring the rate of respiration. Once the mouse was deeply anesthetized, it was placed on an in-house-made stand, the head was immobilized, scalp hair was carefully removed using a hair removing lotion before placing the fiber-optic probe, and a sponge was inserted underneath the chin. Mice's body temperature was kept constant at ~34°C. Core body temperature was monitored continuously during the experiment using a rectal temperature probe (YSI) inserted ~2 cm into the rectum. Other vital systematic parameters, including heart rate and arterial oxygen saturation (SpO_2), were measured simultaneously by pulse oximeter (Nonin, 8600) on the foot. For the induction of brain injury, we used the weight-drop technique by a 50 g weight cylindrical metallic rod falling from ~90 cm height along a metal tube striking the mouse's head. The point of impact was between the anterior coronal suture (bregma) and posterior coronal suture (lambda). This model of injury closely mimics real-life focal head trauma and does not produce apparent structural damage to the brain.[24] Baseline reflectance measurements were obtained prior to induction of injury for 10 min, after which the mouse was removed and placed under the weight-drop device orthogonal to the point of impact. Immediately postinjury, the mouse was returned to the optical setup and the effects of injury were studied 20 min post-trauma. At the end of 20 min, a single injection of neuroprotective drug was administrated intraperitoneally (IP) and measurements were acquired for another 30 min. After 30 min, the mouse was sacrificed. Sham mice ($n = 10$)

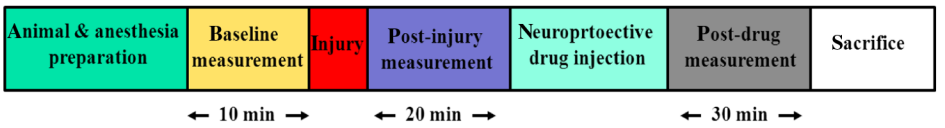

Fig. 1 Experimental protocol.

receiving anesthesia but no injury were used as a control group. All the neuroprotective drugs, hypertonic saline (HTS), mannitol, morphine, melatonin, and minocycline, were purchased from Sigma-Aldrich, Ltd. (Rehovot, Israel). The experimental protocol is outlined in Fig. 1. All animals were handled in accordance with protocol approved by Ariel University Animal Care Committee.

2.2 *Experimental Setup*

The configuration of the experimental setup is displayed in Fig. 2(a). It consisted of two wideband light sources, a bifurcated fiber-optic probe placed in direct contact with the scalp surface, spectrometer, pulse oximeter, rectal probe, and a computer station with control software. The white light bulb inside the first light source (Stockler&Yale, Inc., M1000) was replaced with a broadband quartz-tungsten-halogen lamp (IT, 9596-ER) to provide a smooth continuum broadband spectral profile along the near-infrared (NIR) region and stable intensity over time. Optical fiber ($D = 5$ mm) connected to this light source was placed ~1 mm from the surface of the head (above the right ear). The diffuse light emanating from the brain was delivered to a portable miniature fiber-optic spectrometer (USB4000, Ocean Optics, Dunedin, Florida, USA) via bifurcated fiber with an external diameter of $D = 1.3$ mm, mounted perpendicular to the scalp surface and, hence, orthogonal to the first light source fiber. The bifurcated fiber probe was composed of two branches. One branch is connected to the second white light source (HL-2000-FHSA-LL, Ocean Optics, Inc.) and the other, for light collection to the USB4000 spectrometer. The center-to-center separation between the source and detector fibers inside the probe is ~0.4 mm. The receiver fiber collects the diffuse reflected light in two different modes: in mode 1 (light source #1 = OFF, light source #2 = ON): source–collector separation is SDS = 0.4 mm (sensitive to reduced scattering coefficient, $\mu s'$), and in mode 2 (light source #1 = ON, light source #2 = OFF): source–collector separation is SDS≈ 13 mm (sensitive to absorption coefficient, μ_a). The SDS in mode 2 was approximate via the length of arc formula assuming the brain as roughly spherical in shape. With a mouse brain

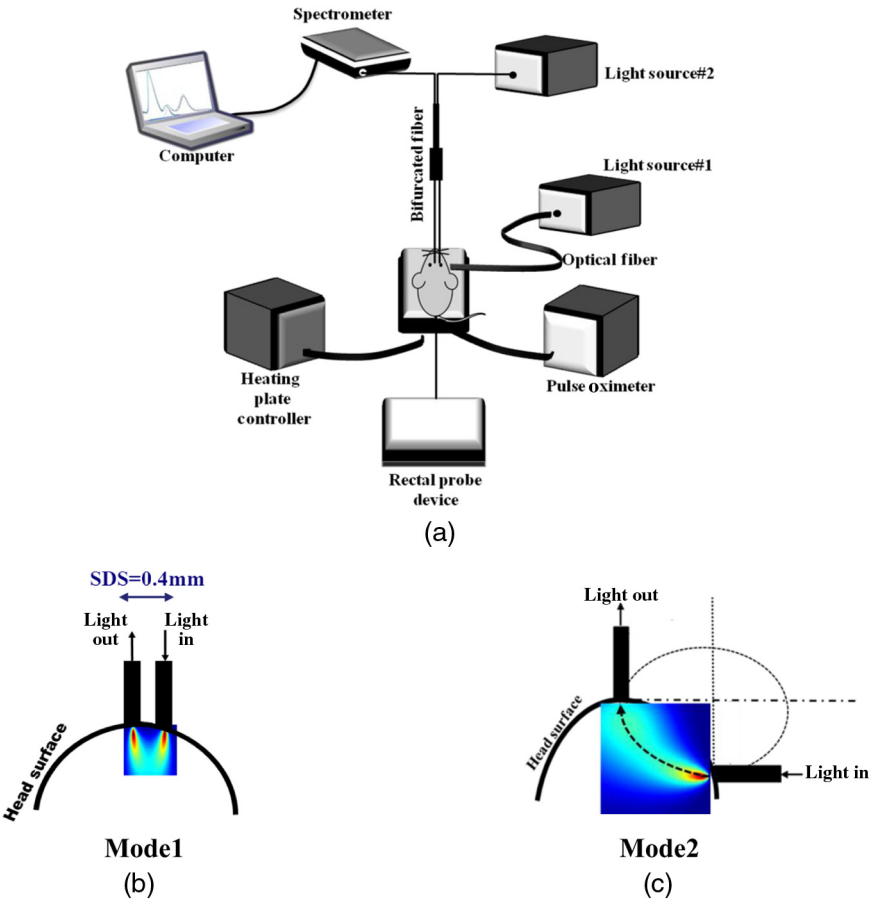

Fig. 2 (a) Schematic representation of system configuration for spectroscopic measurement. Computer simulation of photon migration path distribution from source to detector for (b) mode 1: light source #1 = OFF, light source #2 = ON and (c) mode 2: light source #1 = ON, light source #2 = OFF, respectively.

radius of ~8 mm, the distance between the source and detector is $[(\pi/2) \times R] \approx 13$ mm. Consequentially, at SDS ≈ 13 mm, we achieve relatively deep sampling, while at SDS $= 0.4$ mm, we sample localized volumes (superficial layers). Thus, as the distance between the source and detector decreases, we transition from collection of multiply scattered light to collection of photons that experience few or single scattering events, albeit with a lower chance of absorption. Simulation of light propagation calculated by analytical half-space Green's function of photon diffusion equation[36] is also presented in Figs. 2(b) and 2(c) for each mode of operation, respectively. The banana-shaped photon path profile between the source and detection point are clearly shown in the figures. In both operation modes, the reflected signal is dispersed and detected by the CCD array in the spectrometer. The spectrometer system has a 3648-element linear CCD array (8 μm $\times$ 200 μm, pixel size) with 16-bit resolution, and a spectral range encompassing 200 to 1100 nm. Optical fibers were connected to an x-y-z mechanical stage (Thorlabs, DT12) for position control, and care was taken to ensure gentle contact between the probe arms and the scalp surface throughout the experiments, in order to minimize compression of the local tissues.

2.3 *Calibration*

The measured NIR diffuse light reflectance spectra underwent reflectance calibration, which was performed to compensate for the spectral response of the system and for the dark current of the detector. The spectral response of the system at wavelength λ was characterized by acquiring spectral profile $W(\lambda)$ corresponding to the light reflected from a standard white Spectralon (WS-1, Ocean Optics). Dark response $D(\lambda)$ was characterized by acquiring a spectrum while the light source was turned off and the spectrometer was covered by an opaque black plastic cap. The spectrometer is programmed to automatically subtract a background reading for every reflectance measurement. The acquired spectral and dark responses of the system, obtained before each experiment, were then used to normalize the acquired diffuse reflectance spectrum $R_d(\lambda)$, according to the following equation:

$$\hat{R}_d(\lambda) = \frac{R_d(\lambda) - D(\lambda)}{W(\lambda) - D(\lambda)}. \tag{1}$$

2.4 *Estimation of Optical and Hemodynamic Parameters*

In biophotonics, determination of the optical properties of tissue, namely absorption (μ_a) and reduced scattering ($\mu s'$) coefficients, requires the quantification of both constants' spectral behavior. Importantly, the separation of the absorption and light scattering coefficients enables the accurate quantification of tissue's chemical constituents (related to light absorption), such as hemoglobin concentration and oxygen saturation, as well as its structural properties (related to light scattering). In contrast to the traditional DRS data analysis obtained through multiple SDS and diffusion equations,[37,38] here we employed a different approach to estimate these coefficients. It has already been shown that at low SDS (<1 mm, shallow probing), DRS is highly sensitive to scattering changes in which the detected reflected light is dominated by shorter path-length photons (short depth).[39] On the contrary, at high SDS (>10 mm, deep probing), the detected reflected light is dominated by longer path-length photons (longer depth) and, hence, is more highly sensitive to absorption.[30] Thus, measurements from at least two source–detector distances can result in different sensitivities to absorption and to reduced scattering coefficients, which in turn enable us to independently quantify the optical properties of a sample under investigation. At this point, we want to emphasize that although this methodology is yet to be validated using tissue-simulating phantoms with known optical properties, we intend in the near future to investigate this setup further and to evaluate its performance in comparison to other DRS systems with a set of phantoms having different optical properties. The following steps were used to extract tissue properties.

Step #1: Reduced scattering coefficient $\mu_s'(\lambda)$ was assumed to be a function of the wavelength obeying the power law dependence in the following form (commonly employed for tissue optics):[40]

$$\mu_s'(\lambda) = A\lambda^{-\mathrm{sp}}, \tag{2}$$

where $\mu_s' = \mu_s(1-g)$ is the reduced scattering coefficient, g is the anisotropy factor, and μ_s represents the scattering coefficient. A is the scattering amplitude, which is related to the density of the scatterers (cell membrane, organelle membrane, cell nuclei, and other intracellular organelles, including the mitochondria), their distribution, and refractive index changes, whereas sp is the scattering power (exponent) depending on the average scatterer size of the medium and defines the spectral behavior of the reduced scattering coefficient.[41] Together, A and sp convey morphological and functional information of biological tissue. As mentioned above, since light collected at a short source–detector distance is insensitive to variation in absorption and concomitantly very sensitive to light scattering changes, it can be said that[42]

$$\mu_s'(\lambda)_{|_{\mathrm{SDS<1\ mm}}} \propto \hat{R}_d(\lambda). \tag{3}$$

Thus, Eq. (3) can be retrieved by collecting the diffuse light within mode 1.

Step #2: To estimate the absorption coefficient $\mu_a(\lambda)$, mode 2, we utilized the following modified Beer-Lambert law[43] by measuring the spatial variation of the normalized diffuse reflectance:

$$\mu_a(\lambda)_{|_{\mathrm{SDS>10\ mm}}} \propto \frac{-\log_{10}[\hat{R}_d(\lambda)]}{L}, \tag{4}$$

where $L = d \times \beta(\lambda)$, d is the physical distance between the source and detector spacing in mode 2 and $\beta(\lambda)$ is a path-length factor, which accounts for increases in the photon path length caused by tissue scattering.[44] λ is the wavelength of light.

Step #3: Analysis of collected absorption spectra can be used to identify and quantify the presence and concentration of chromophores in tissue. Therefore, once $\mu_a(\lambda)$ is recovered based on Eq. (4), main tissue composition parameters in the NIR region, such as oxyhemoglobin (HbO_2), deoxyhemoglobin (Hbr), total hemoglobin concentration (THC $= HbO_2 + Hbr$), hemoglobin oxygen saturation [$StO_2 = (HbO_2/THC) \times 100$], water concentration ($H_2O$), and lipid (fat) percentage, can be determined by using Moore-Penrose pseudoinverse algorithm to $\vec{\mu}_a(\lambda) = [\varepsilon(\lambda)]\vec{c}$:

$$\vec{c} = [\varepsilon(\lambda)]^T\{[\varepsilon(\lambda)][\varepsilon(\lambda)]^T + \beta[I]\}^{-1}\vec{\mu}_a(\lambda) \cdot \vec{k}, \tag{5}$$

where $\vec{c}$ is the chromophore (absorber) molar concentration, $\vec{\mu}_a(\lambda)$ is the calculated absorption coefficient derived from Eq. (4) of length N, and $[\varepsilon(\lambda)]$ matrix is the molar spectral absorbance coefficient of an absorbing chromophore at wavelength λ with size $N \times M$:

$$[\varepsilon(\lambda)] \equiv \begin{bmatrix} \varepsilon_{HbO_2}(\lambda_1) & \varepsilon_{Hbr}(\lambda_1) & \varepsilon_{lipid}(\lambda_1) & \varepsilon_{H_2O}(\lambda_1) \\ \varepsilon_{HbO_2}(\lambda_2) & \varepsilon_{Hbr}(\lambda_2) & \varepsilon_{lipid}(\lambda_2) & \varepsilon_{H_2O}(\lambda_2) \\ \vdots & \vdots & \vdots & \vdots \\ \varepsilon_{HbO_2}(\lambda_n) & \varepsilon_{Hbr}(\lambda_n) & \varepsilon_{lipid}(\lambda_n) & \varepsilon_{H_2O}(\lambda_n) \end{bmatrix}, \tag{6}$$

where ε_i is the extinction coefficient of a particular chromophore at a given wavelength (λ). $\vec{k}$ is the proportionality coefficient vector of length M that is related to *a priori* known concentration levels. The upper letter T represents the transpose matrix and upper number -1 denotes inverse of the matrix. $[I]$ is identity (or unit) matrix and β is the regularization parameter proportional to $\beta \propto \max\{[\varepsilon(\lambda)][\varepsilon(\lambda)]^T\}$.[45] Routinely, the constraint that is usually employed is a positive value of concentration. We assume that the influence of other absorbing molecules, such as melanin, collagen, cytochtome-*c* oxidase, etc., lying within these wavelengths is negligible in comparison to hemoglobin, lipid, and water levels. In addition, since the mouse layers are optically thin (skull ~ 500 μm, brain ~ 1 cm, etc.), the derived values of optical properties and chromophore responses will be considered to be average values resulting from sampling bulk volume.

2.5 *Data Acquisition and Processing*

Data acquisition, performed every 60 s during the entire protocol (60 min), was accomplished using spectrometer software displaying the reflectance spectrum within the range of 650 to 1000 nm, by 2-nm increments, in real time. The spectrometer interfaces to a desktop computer (Intel Core, E6750 Processor running at 2.67 GHz with 2 GB memory) via USB 2.0 port and is controlled by the Ocean Optics software (OOI Base 32). Each set of acquired data includes the measurements of replicate spectra (total of $n = 20$) at the rate of 4 Hz during a single data collection session. Thus, the data acquisition time for one measurement corresponds to 5 s. These spectra are later assembled together to a single average spectrum increasing the signal-to-noise ratio by a factor of $\sqrt{n}$. After the DRS data acquisitions are completed and stored in the computer, their analysis through Eqs. (1)–(6) was carried out off-line using in-house scripts written in MatLab® software (The MathWorks, Inc., Natick, Massachusetts, USA) on a 2.3 GHz Intel(R) Core™ i5 CPU, 4 GB RAM laptop.

2.6 *Statistical Analysis*

Results are presented as mean $\pm$ standard error, and the Student's t test was performed to determine significant differences. Results were judged to be significant if the p value was <0.05. Mann-Whitney U test was also performed and results were similar to the t-test data. Calculations were done via Matlab®'s Statistic Toolbox.

3 Results and Discussion

3.1 *Experiment #1: Hypertonic Saline Test*

3.1.1 *Introduction*

HTS is an osmotic agent administered IP to patients in the acute phase of severe TBI. HTS acts to reduce brain swelling by increasing the sodium levels in the blood stream, thereby inducing a shift of fluid across the osmotic gradient it generates from the intracellular to the extracellular space. Shortly after administration, HTS reduces blood viscosity, increasing the rheological properties, which improves cerebral blood flow (CBF) and cerebral oxygenation, causing autoregulatory vasoconstriction, thereby reducing intracranial pressure (ICP).[46–48]

3.1.2 *Results*

Figures 3(a)–3(c) show the dynamic time courses presented by bar graphs, which represent the average and standard error of chromophore concentration of mice ($n = 10$) at the following three states: baseline [Fig. 3(a)], following brain injury [Fig. 3(b)], and after HTS administration [Fig. 3(c)]. 23.4% NaCl HTS (Ref. 49) was injected IP 20 min after induction of injury. In the results presented in Fig. 3(a) of baseline, no significant fluctuations over time in brain parameters are observed, which reflects stability in measurements. Relative to baseline, a difference in brain chromophore levels was demonstrated following injury [Fig. 3(b)]. Specifically, a decrease in HbO_2, THC, and StO_2 was observed over time, concurrently with $\sim$11% increased Hbr. Assuming that the concentration of red blood cells (hematocrit level) remains constant following injury, THC can be used as a surrogate marker of CBF. Reduced CBF following brain trauma observed here is consistent with our previous studies[34,35] and stands in agreement with results of neuroimaging studies, which revealed heterogeneous regional disturbances of CBF.[50–52] Under decreased CBF, brain cells undergo a series of pathophysiologic changes further complicated by decreased oxygen supply, as reflected in lowered StO_2, contributing to secondary injury.[53] Reduced StO_2 indicates decreased oxygen delivery to the brain and failure of cellular respiration that can lead to permanent brain damage, neurological disorders, or even death. Altogether, these results reflect the pathophysiology of the brain following trauma and agree well with other documented studies.[54,55] Since the trend in Fig. 3(a) was consistent among all mice examined, in the following treatment results (Figs. 4 and 5), we will ignore the baseline graph. In Fig. 3(c), the effect of HTS administration is shown: HbO_2 and THC were slightly increased (return to baseline afterward), while no significant change in Hbr and StO_2 was shown. Figure 3(d) displays the variation in the normalized reduced scattering spectra (i.e., μ_s' versus λ) measured for the above three states. Each line is the average over time in measurements of baseline (10 min), following injury (20 min), and post-HTS injection (30 min), respectively. As mentioned in Sec. 2.4, scattering slope (sp) can serve as a marker of the structural changes occurring in brain tissue subsequent to TBI. As seen in Fig. 3(d), progress from a normal brain (baseline) to an injury state is marked by an sp decrease of $\sim$18% (0.9 to 0.74), demonstrating the morphologic changes occurring in the brain, attributed to the cellular swelling within brain structures. Surprisingly, sp did not return toward its baseline level nor did it increase following HTS injection (30 min) (sp = 0.68). At the same time, in comparison to our previous studies using the

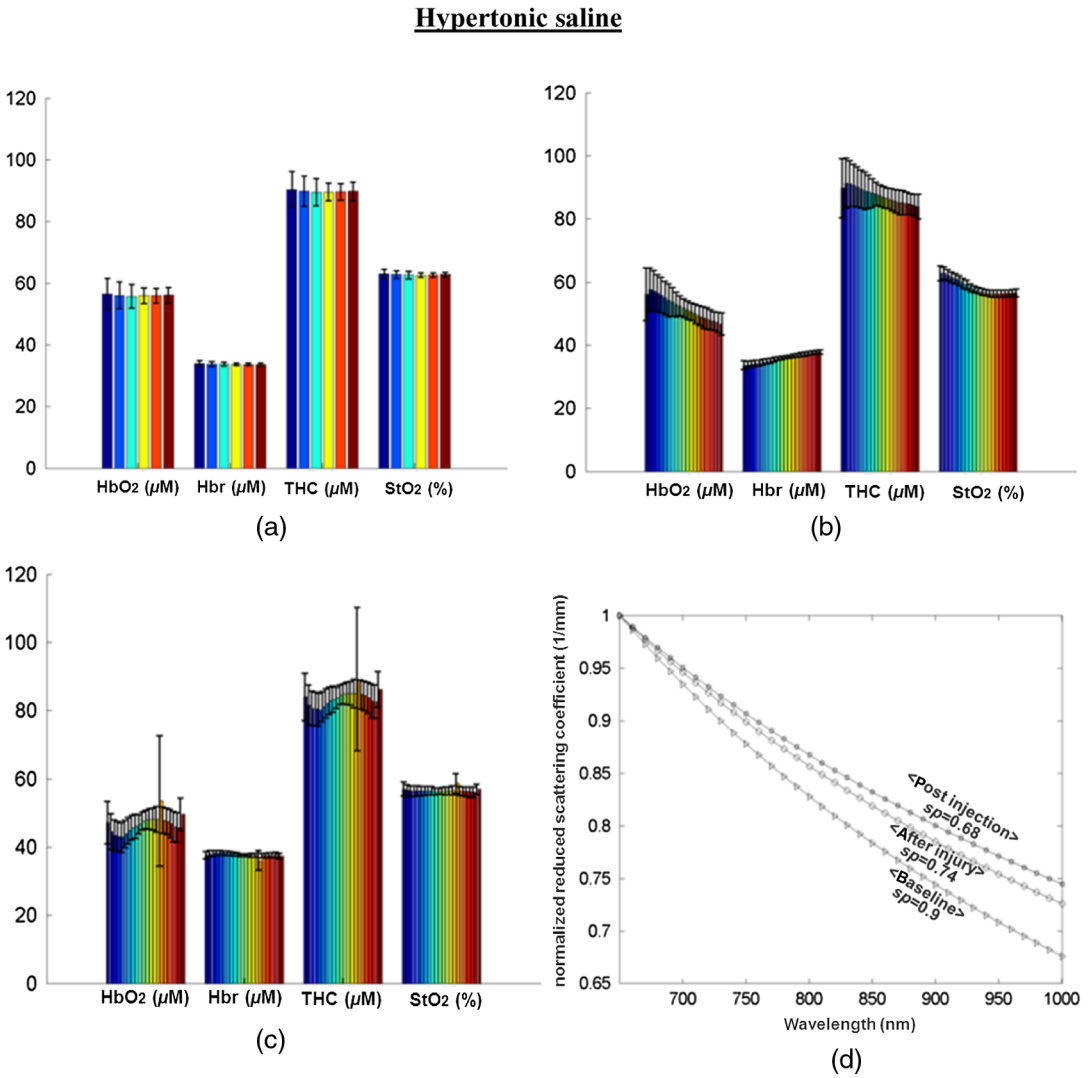

Fig. 3 Bar graph of chromophore concentrations at three states: (a) preinjury (baseline), (b) postfocal traumatic brain injury (TBI), and (c) following hypertonic saline (HTS) administration given immediately 20 min after the injury. The trend in chromophore following these three states is clearly observed. Each bar represents the average and standard error over 10 mice. In (a), each bar corresponds to 2 min, while in (b) and (c), it corresponds to 1 min. (d) Average normalized reduced scattering spectra for the above three states. Slope (sp) decreased by ~18% from normal brain (baseline) and did not return toward its baseline level after HTS injection. However, it delays or prevents further decrease of sp.

same animal TBI model and optical setup (Ref. 34, Fig. 3 and Ref. 35, Fig. 8), it can be said that HTS did delay a gradual decrease of sp seen without HTS injection. The nonadvancement of cellular swelling, together with almost no change in cerebral water accumulation [Fig. 7(a)], suggest a stabilizing effect of HTS upon ICP, as reported elsewhere.[47,56,57]

3.2 *Experiment #2: Morphine Test*

3.2.1 *Introduction*

Morphine, commonly used in patients suffering head trauma, is an opioid analgesic drug used to relieve intense pain and suffering. Once injected, morphine enters the blood stream, which carries it to the brain and other parts of the body where it acts primarily as an agonist of the μ opioid receptors in the central nervous system and in peripheral tissue.[58–60] Recently, Holbrook et al. demonstrated that the administration of morphine for optimal control of pain and anxiety after injury may reduce the risk of post-traumatic stress disorder.[61]

3.2.2 *Results*

Figures 4(a) and 4(b) show the average dynamics of chromophore concentration of 10 mice ($n = 10$) during injury [Fig. (4a)] and after IP morphine administration [Fig. (4b)] at a dose of 10 mg/kg of body weight,[59] 20 min after injury. As can be seen in Fig. 4(b), morphine worsens the hemodynamic reaction; there is a content stabilization and then ~15 min after the injection, a decrease in levels of HbO_2, THC, and StO_2 is observed. On the other hand, morphine succeeds in maintaining the Hbr level. These findings are opposed to those obtained by de Nadal et al., who found morphine to have no significant effect on cerebral hemodynamic content and blood flow in severe brain injury patients.[62] In Fig. 4(c), variation in the normalized

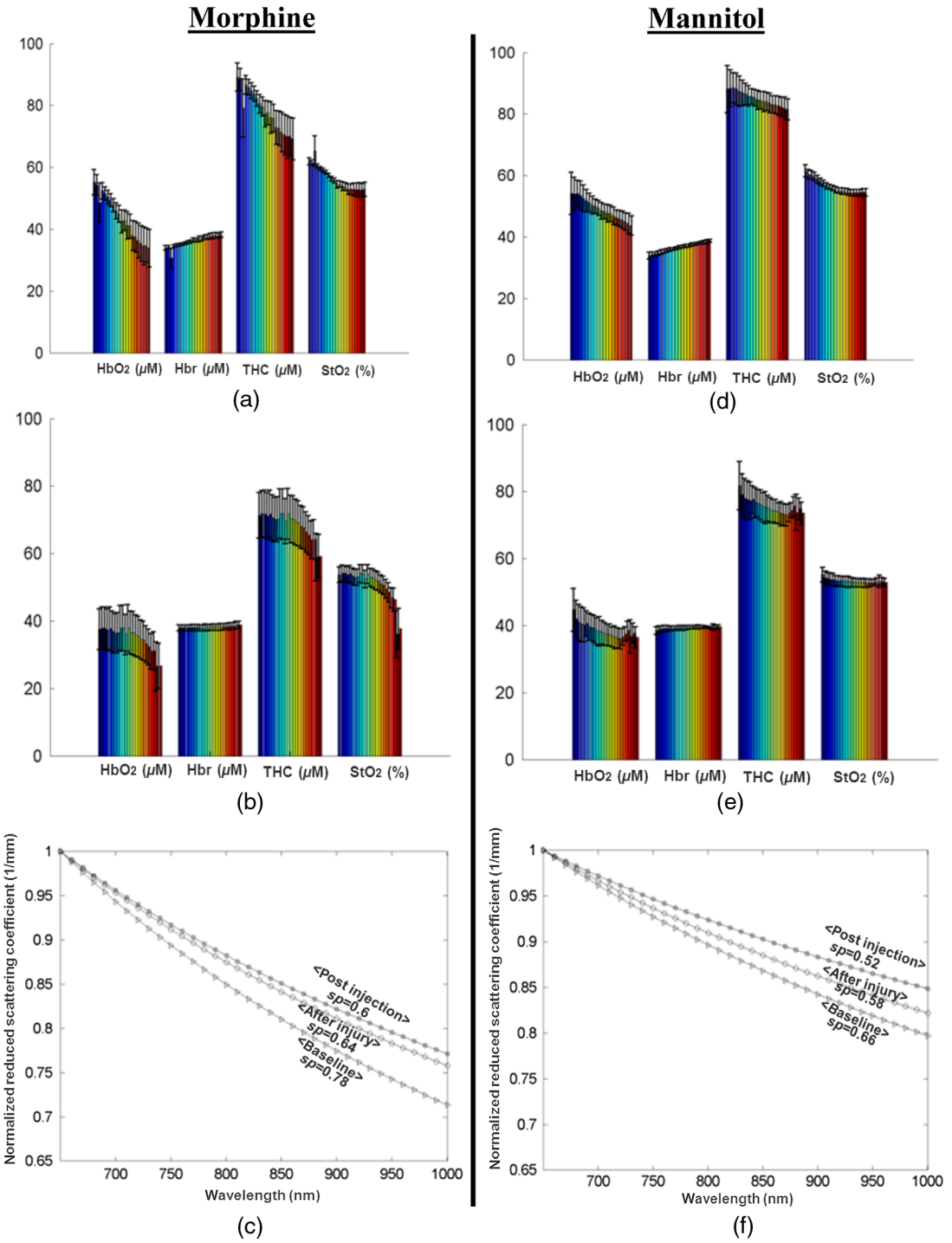

Fig. 4 Bar graph of chromophore concentrations postfocal TBI (a) and following morphine administration (b). Each bar represents the average and standard error over 10 mice over 1 min. (c) Average normalized reduced scattering spectra for the above two states. (d) to (f) The same for mannitol experiment.

reduced scattering spectra is presented as in HTS [Fig. 3(d)]. Each line is the average over time in measurements of the baseline (10 min), following injury (20 min), and postmorphine injection (30 min), respectively, from 10 mice. As seen, after treatment with morphine, sp did not return to its baseline level or increase following morphine injection. Thus, it appears that morphine was able to delay or prevent the gradual decrease of sp seen in untreated TBI.[34,35] This delay in cell swelling, probably reflecting a decrease in ICP, is in agreement with Lauer et al., who reported that morphine administration preserves systemic arterial pressure without elevating ICP in head injury patients.[63] It should be stressed that the clinical effectiveness of morphine for the reduction of ICP in severe head injury remains open to question.[63,64]

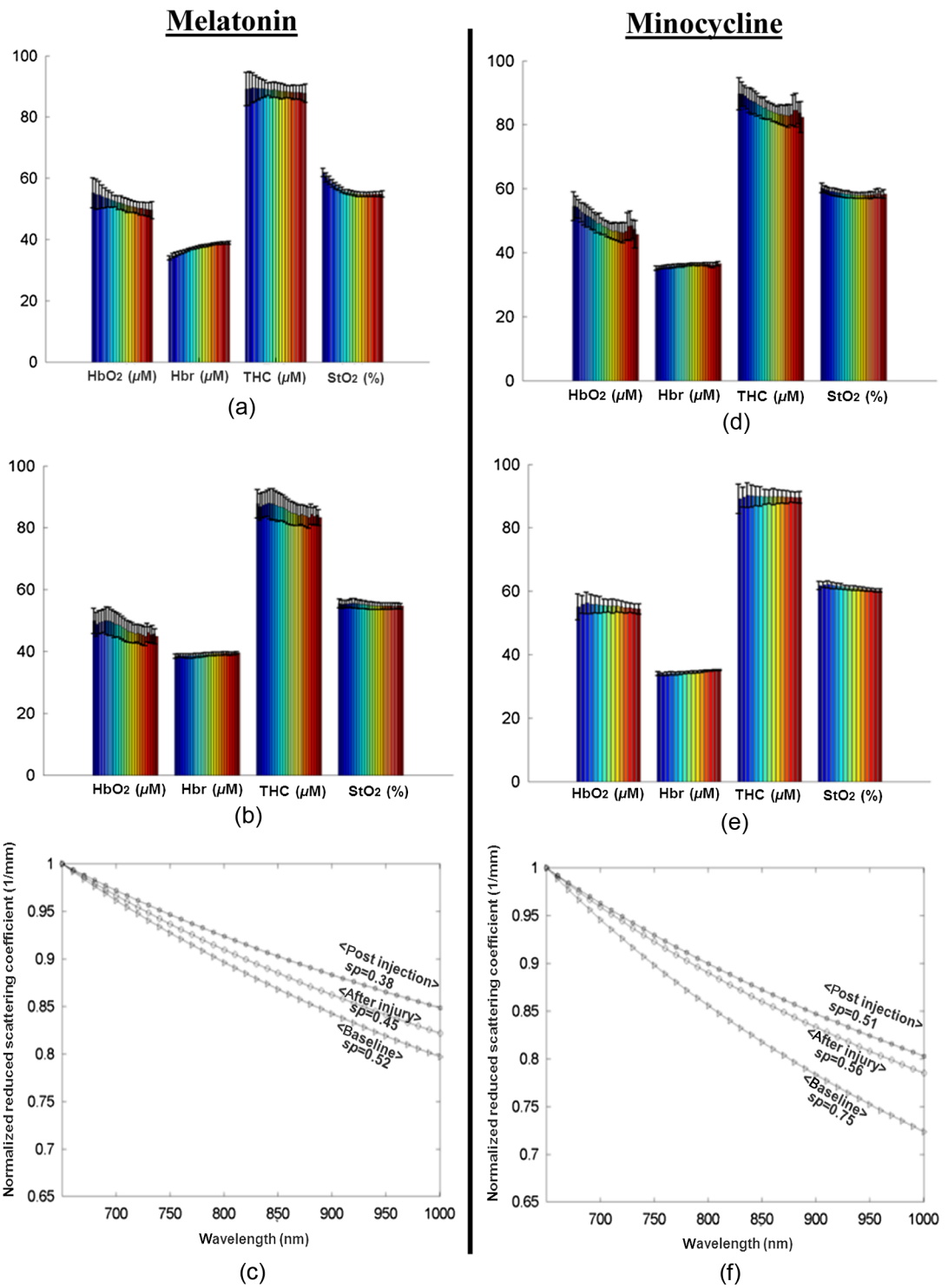

Fig. 5 The same as in Fig. 4 for melatonin [(a) to (c)] and minocycline [(d) to (f)] studies.

3.3 *Experiment #3: Mannitol Test*

3.3.1 *Introduction*

Mannitol is a sugar-alcohol solution which is somewhat effective in reducing brain swelling and controlling ICP in TBI patients. Mannitol is also used in the treatment of large-scale cerebral occlusive diseases.[65] The presumed mechanisms include osmotic dehydration, shrinkage of brain parenchyma, and improvement of the blood's rheological properties to improve CBF.[66] Nonetheless, its effectiveness in the ongoing treatment of severe head injury remains under dispute.[67–69] There is evidence that excessive administration of mannitol may be harmful.[67]

3.3.2 *Results*

Figures 4(d) and 4(e) show the average dynamics of chromophore concentration of 10 mice ($n = 10$) during injury [Fig. (4d)] and after IP mannitol administration [Fig. (4e)] at a dose of 2 mg/kg

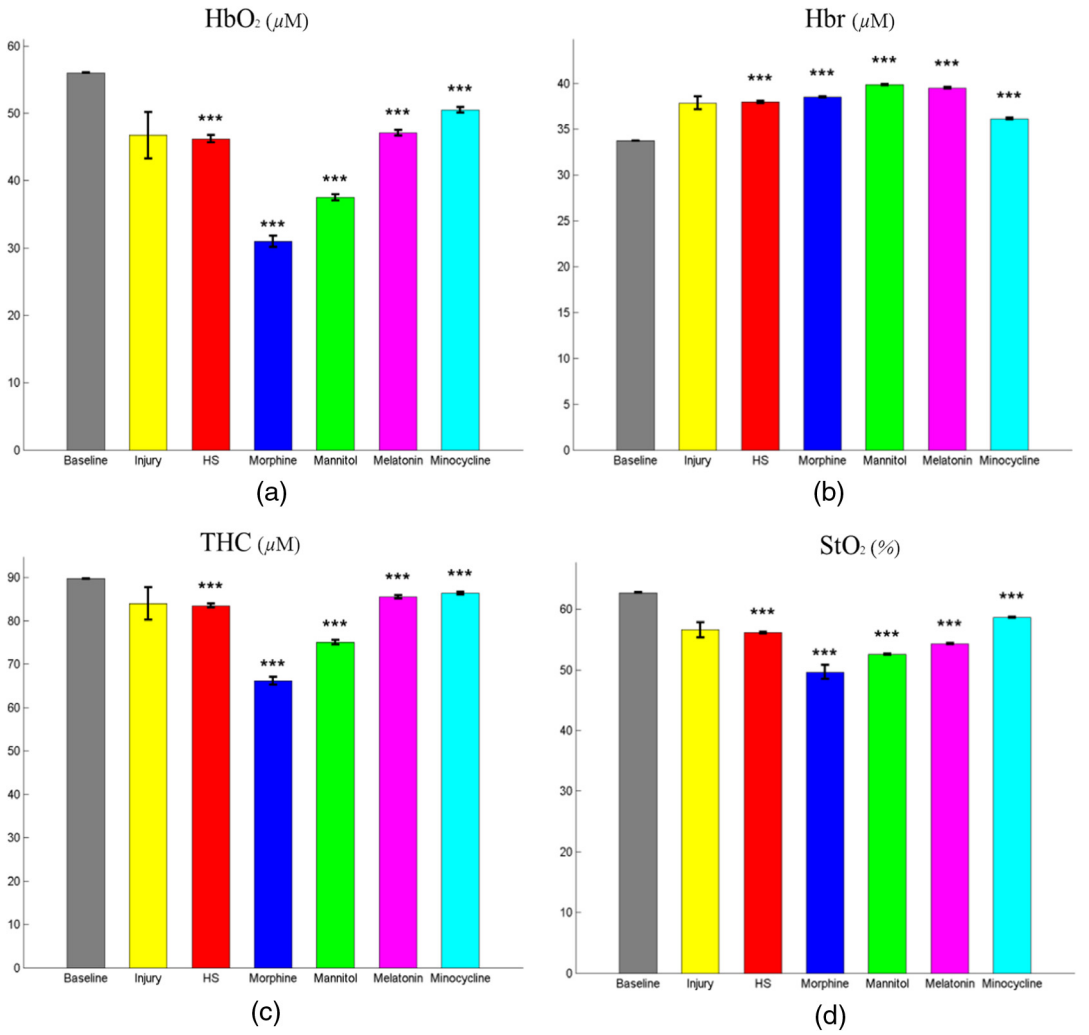

Fig. 6 Summary of the drugs' differential effects upon chromophore response. Each panel includes the mean ± standard error (SE) of baseline chromophore concentrations, their levels 20 min postinjury, and status during the 30 min of measurements following drug injection. ***Significant difference between drug administration with injury state ($p < 0.001$).

of body weight,[70] 20 min after induction of injury. Following mannitol injection, a decrease in HbO_2, THC, and slightly of StO_2 was observed over time, concurrently with a slightly increased Hbr. In Fig. 4(f), variation in the normalized reduced scattering spectra is presented. Each line is the average over time in measurements of baseline (10 min), following injury (20 min), and post-HTS injection (30 min), respectively, from 10 mice. As before, sp did not return to its baseline or increase following mannitol administration. Thus, it appears that mannitol was effective in delaying or restricting the postinjury decrease in sp. This delayed cellular swelling apparently reflects the effectiveness of mannitol in the modulation of ICP.[71]

3.4 *Experiment #4: Melatonin Test*

3.4.1 *Introduction*

Melatonin (5-methoxy-N-acetyltryptamine) is a methoxyindole hormone produced by the brain's pineal gland, whose physiological roles include protecting the cellular membrane from oxidative agents.[72,73] It is a highly efficient free radical scavenger found to be of value in the treatment of cardiovascular diseases, degenerative brain diseases, brain injuries, stroke, and numerous cancers.[74,75] Melatonin was also shown to induce neuroprotective effects by increasing the activity and expression of the antioxidant enzymes superoxide dismutase, glutathione peroxides, and glutathione reductase under both baseline physiological conditions and under elevated oxidative stress.[76,77] Previous studies have shown that melatonin administration after TBI reduces contusion volume and attenuates neurobehavioral dysfunction, moderating the level of brain tissue damage, along with a reduction in inflammation and the rate of infections.[78,79]

3.4.2 *Results*

Figures 5(a) and 5(b) show the average dynamics of chromophore concentration of 10 mice ($n = 10$) during injury [Fig. (5a)] and after melatonin administered IP [Fig. (5b)] at a dose of 10 mg/kg of body weight,[77] 20 min after induction of injury. The effect of injury on the brain is clearly seen in Fig. 5(b); a decrease in HbO_2 and StO_2 was observed over time, concurrently with an increased Hbr. Following injection, Fig. 5(b), melatonin stabilized Hbr and StO_2 hemodynamics, and caused a moderate decrease in HbO_2 and THC, inhibiting further brain damage. In Fig. 5(c), variations in the normalized reduced scattering spectra measured for the three states are

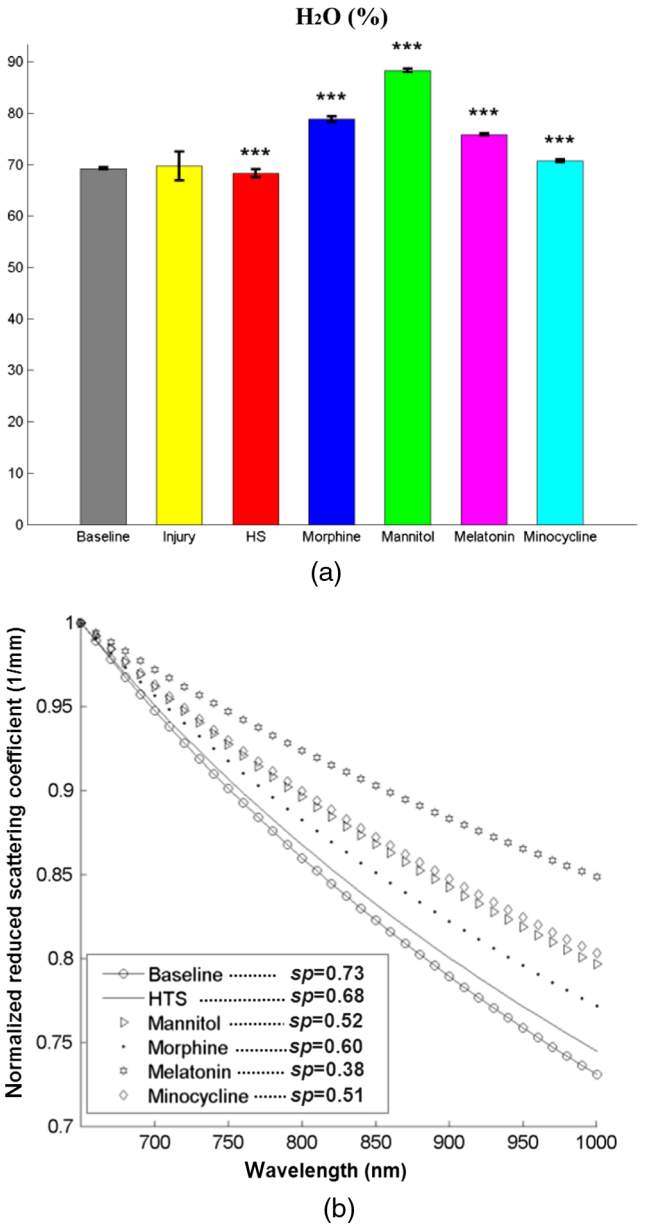

Fig. 7 (a) The measured average value of brain water content over 30 min following drug injection. The results are expressed as the mean ± SE. ***Significant difference between drug administration with injury state ($p < 0.001$). (b) Spectral differences between the drugs' effects and in comparison to baseline state (normal brain). Each spectrum represents the average during 30 min after drug administration.

presented. Each line is the average over time in measurements of baseline (10 min), following injury (20 min), and post-HTS injection (30 min), respectively, from 10 mice. Overall, the slope did not return to its baseline or increase, suggesting an increase in ICP.[80] Very recently, Dehghan et al. reported the effect of melatonin on ICP and brain edema following TBI in rats a using weight-drop model.[81] They concluded that daily administration of melatonin for 72 h after TBI is effective in decreasing ICP and brain edema, improving neurological scores. A possible reason for this discrepancy with the present study could be the difference in dose and timing of melatonin administration, injury model, and measurement setup. Nonetheless, other studies also showed reduced brain edema[82,83] and its effectiveness in diverse models of experimental traumatic central nervous system.[74,84,85]

3.5 *Experiment #5: Minocycline Test*

3.5.1 *Introduction*

Minocycline (minocin), a semisynthetic tetracycline antibiotic, is a multifaceted therapeutic agent potentially effective in the treatment of neurological disorders, including stroke, multiple sclerosis, TBI, spinal cord injury, neurodegenerative diseases (Huntington, Parkinson), and more.[12,86–89] Minocycline exerts its neuroprotective effects via suppression of cerebral inflammation and apoptotis and by stabilizing levels of soluble alpha-amyloid precursor protein.[90,91]

3.5.2 *Results*

Figures 5(d) and 5(e) show the average dynamics of chromophore concentration of 10 mice ($n = 10$) during injury [Fig. (5d)] and after IP minocycline administration [Fig. (5e)] at a dose of 45 mg/kg of body weight,[92,93] 20 min after injury. The effect of injury on the brain is clearly seen in Fig. 5(d), a decrease in HbO_2, THC, and StO_2 concurrently with increased Hbr. Following injection, Fig. 5(e), minocycline treatment caused stabilization in chromophore levels. Figure 5(f) presents the variation in normalized reduced scattering spectra, whose slope did not return to its baseline or increase. The decrease in sp may be attributed to increased BBB permeability induced by minocycline, leading to cerebral edema and increased ICP.[94,95]

For the purpose of comparison, Figs. 6 and 7 provide a summary of the drugs' differential effects upon chromophore and structural (scattering) parameters, derived from the previous figures. In Fig. 6, each panel includes baseline chromophore concentrations, their average levels 20 min after injury, and status during the 30 min following drug injection. By comparing the panels, it is evident that the drugs differentially affected brain hemodynamics, which were markedly altered by injury ($p<0.001$). Specifically, HTS, melatonin, and minocycline partially stabilized chromophores' concentrations toward their baseline levels, thereby mitigating injury pathophysiology and reducing tissue damage. In Fig. 6(a), melatonin and minocycline are shown to increase HbO_2 concentrations toward their baseline level, while no change in HbO_2 level was observed after injury with HTS treatment. Along the same line, in Fig. 6(b), we found that Hbr was slightly increased after drug treatment, except in the case of minocycline, which returned Hbr levels to within the baseline range. Furthermore, Figs. 6(c) and 6(d), deduced from the HbO_2 and Hbr concentration profile (Sec. 2.4), highlight the contribution of each neuroprotectant drug to blood flow (indirectly) and tissue oxygen saturation (StO_2), respectively. Among others, minocycline treatment demonstrated an improvement in blood flow and cerebral oxygenation. In light of these results, it is concluded that minocycline most efficiently reduced brain tissue damage and inhibited the progression of injury by restoring THC to its baseline level and by elevating oxygen saturation. Previous studies have revealed that minocycline successfully reduced brain damage and inflammation, protected against neurogenerative diseases, and improved cognitive functioning.[12,90] As a second alternative to minocycline, it can be argued that HTS had a positive effect on the brain as it mitigated further deterioration of

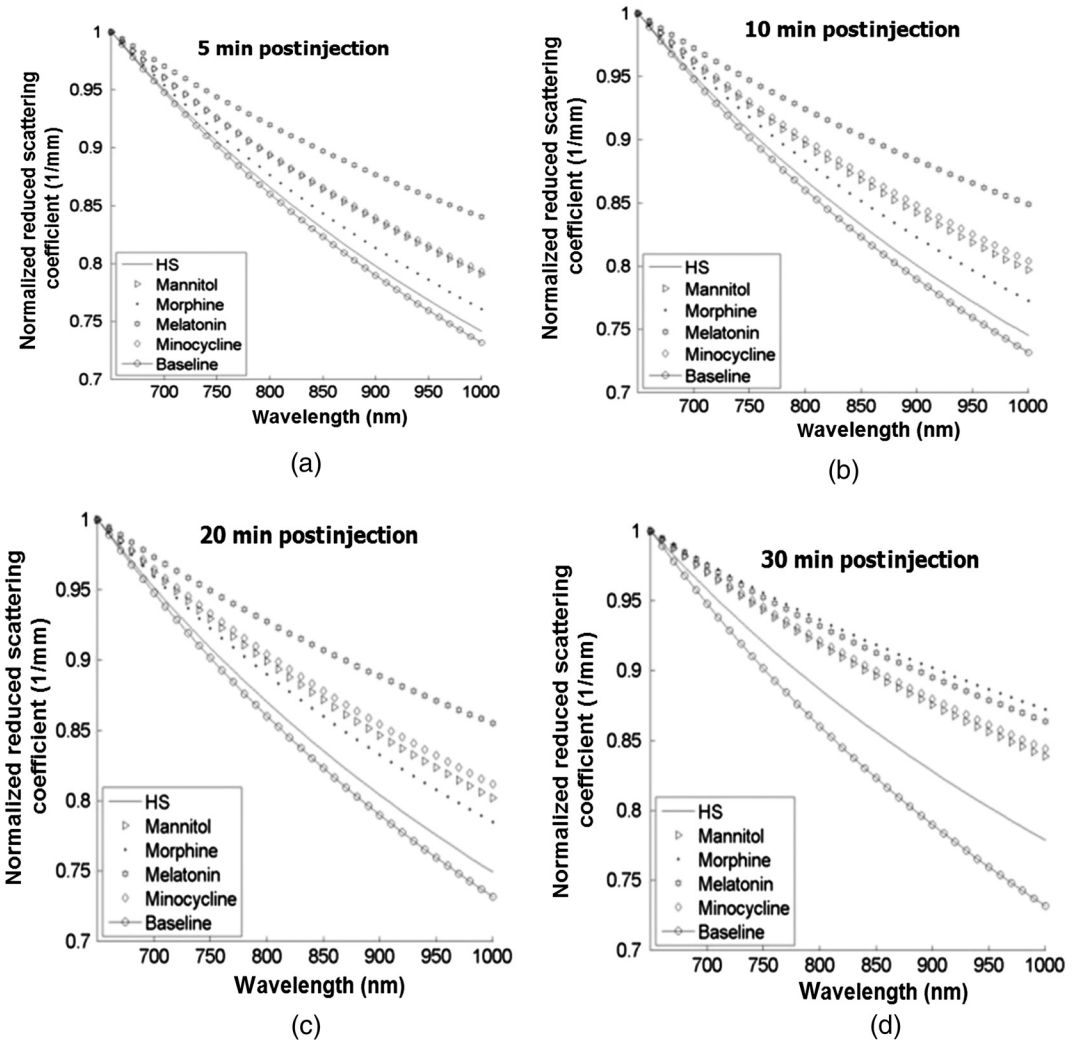

Fig. 8 Normalized reduced scattering spectra following drug therapy at four representative time points. Discrepancies in response of each drug over time are clearly observed highlight brain structural changes to a specific treatment.

injury. Finally, in comparison to other drug treatments, it is clear that notable differences exist with morphine and mannitol, as both drugs failed to recover hemodynamic parameters. Specifically, their negative influence on HbO_2 level is noticeable. The low level of oxygenation induced by morphine [Fig. 6(d)] probably reflects respiratory depression, one of morphine's adverse effects.[96,97]

As mentioned previously, cerebral edema and the associated increase in ICP are the major immediate consequences of TBI that contribute prominently to early postinjury death. Thus, we investigated this causal relationship. Figure 7(a) represents the average brain water concentration during 30 min after drug injection, while Fig. 7(b) presents the average of the normalized reduced scattering coefficient over 30 min postinjection. It is clearly evident from Fig. 7(a) that HTS is the only drug found to decrease cerebral water content after injury toward its baseline level, while minocycline successfully inhibited any further increase in water level after administration.[94] Unexpectedly, morphine and mannitol were found to increase water level by ~7 and 15%, respectively, from normal brain condition. The high dose of mannitol given in the experiment probably passes from the bloodstream into the brain, where it increases ICP, worsening brain swelling.[67,98] However, it is unlikely that water level will increase as such within a short time postinjection. This abnormal behavior should be further elucidated in future study to offer a more complete understanding of mannitol's effects upon cerebral water content. The increase in water content following morphine therapy is also not clear, and this mechanism needs to be further clarified in the future. Our literature search did not reveal such variations in cerebral water concentration after morphine injection in a mouse model of focal TBI.

As stated above, the slope of the graph (sp) represents tissue morphological (cell organelle size, density, distribution, etc.) changes: as the slope increases, returning toward baseline, it reflects a decrease in particle size and *vice versa*. This reduction in sp is attributed to a reduction in cellular swelling and, ultimately, a reduction in ICP. The spectral differences between the drugs' effects in Fig. 7(b) emphasize this point. From both Figs. 7(a) and 7(b), it can be concluded that HTS therapy is the most effective treatment agent for the inhibition of cellular swelling and the moderation of ICP of the injured brain. Our results stand in agreement with other studies that confirmed the beneficial effects of HTS administration upon brain water

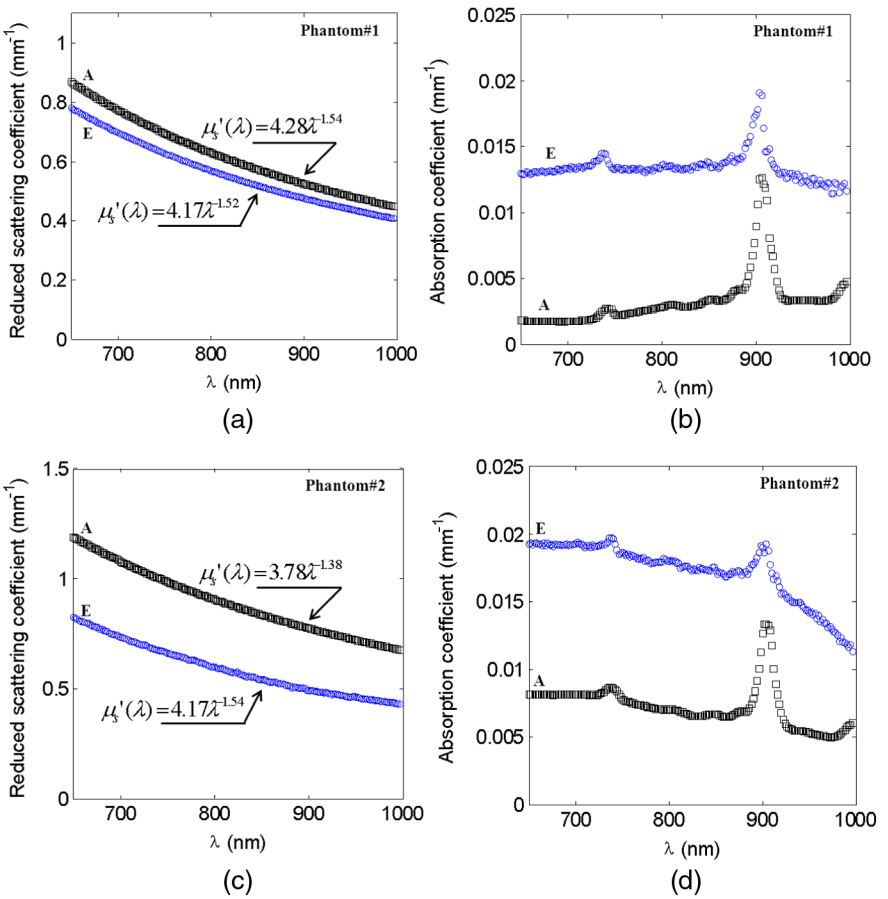

Fig. 9 Estimated reduced scattering (a) and absorption (b) spectra versus the actual (reference) spectra of phantom #1. (c) and (d) Estimated reduced scattering and absorption spectra, respectively, versus the actual (reference) spectra of phantom #2. Note: in all panels, A, actual; E, estimated.

content and ICP, both in humans and in a variety of brain injury paradigms in animals.[47,57,99] In Fig. 8, the normalized reduced scattering spectra under different time intervals are provided for all tested drugs, highlighting the structural trends (slope variations) occurring in the brain during injury and after drug administration in comparison to baseline. Please note the superiority of HTS over the others by increasing the sp (slope becomes closer to baseline). These structural trends describe an increase in particle size or the evolution of swelling of the cells and cell organelles in the brain due to ion and water movements, membrane breakdown, and capillary changes. This figure also demonstrates our ability to follow changes over time in order to monitor cellular swelling within brain structure in high time resolution [Ref. 34, Fig. 7].

In addition to the above animal study, calibration and validation experiments were conducted with different solid-tissue phantoms with known optical properties over the wavelength range of 650 to 1000 nm. In total, one phantom for calibration and two phantoms for validation purposes were used. Following the calibration process, a scale factor (vector) was determined for the true values of scattering and absorption coefficients, respectively. These factors were used later for estimation of the true optical properties of the validation phantoms. Reconstruction of the estimated reduced scattering and absorption spectra versus the actual (reference) spectra of the validation phantoms are shown in Figs. 9(a) and 9(b), respectively. Comparison of $\mu_s'(\lambda)$ in Fig. 9(a) indicates good agreement between the actual and estimated spectra, with small differences in both scattering amplitude (A) and power (sp). Frequently, the normalized reduced scattering spectra are presented and the value of the sp most importantly reflects cellular swelling; with that, a difference of only ~1% in sp was found in phantom #1. At the same time, a difference of ~10% in the estimated sp and A was also observed in comparison to the given values for the second homogenous phantom [Fig. 9(c)]. Normalized reduced scattering coefficient of both phantoms, respectively, is shown in Fig. 10, demonstrating a good correlation between sets of measurements. This observed agreement validates the present method for estimating reduced scattering parameters from the measured diffuse reflectance. On the other hand, the recovered (estimated) absorption spectra profile for both phantoms is illustrated in Figs. 9(b) and 9(d), respectively. Although the intensities of these two recovered absorption spectra are distinct from the true values, their spectral shapes are quite similar. From Eq. (4), it is obvious that the accuracy and magnitude of the absorption measurements depend on the medium pathlength factor. We, therefore, believe that with the larger set of phantoms having different optical properties, an optimal scale vector can be obtained, further reducing the discrepancies (bias) in absorption intensities. Thus, although the absorption spectrum enables quantification of different chromophores' concentration values, in Eq. (5) we used a vector based upon *a priori* knowledge regarding baseline absolute concentration levels in order to compensate for the error derived from the estimated absorption.

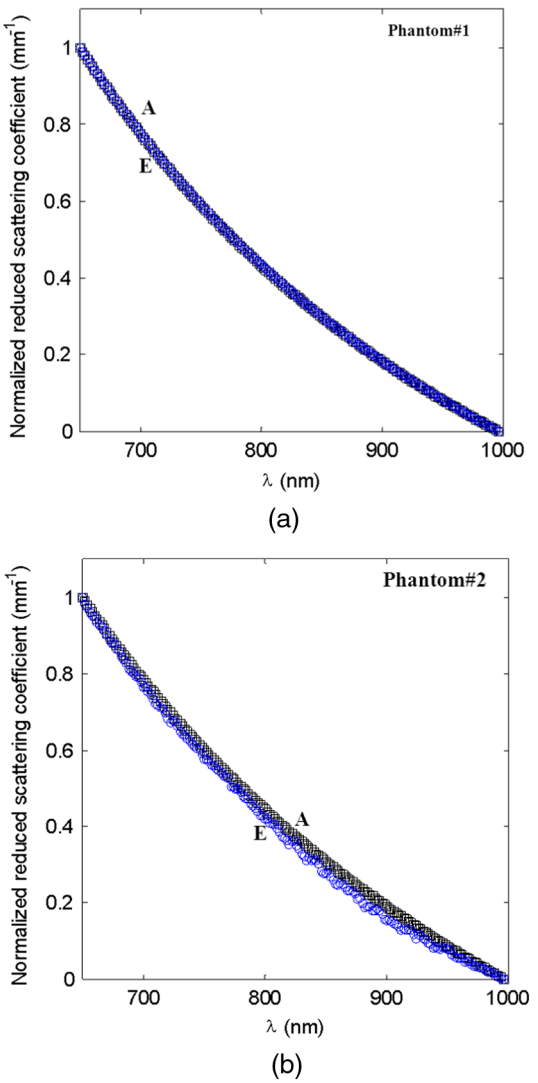

Fig. 10 Estimated (E) and actual (A) normalized reduced scattering spectra of phantom #1 (a) and phantom #2 (b).

4 Conclusion

The primary aim of this study was to evaluate and compare the effects of five different neuroprotective drugs as treatments of head injury in mice using noninvasive optical diffused light spectroscopy. To our knowledge, the present results demonstrate, for the first time, on the macroscopic level the recovery of brain hemodynamic and morphologic parameters induced by drug administration shortly after focal TBI (CHI model). In addition, the global effects of the drugs tested upon this battery of hemodynamic parameters of brain damage were yet to be comparatively quantified.

Taken together, the current results demonstrate that administration of minocycline improved hemodynamic outcome and reduced the level of tissue injury at an early phase postinjury (~1 h), while HTS administration decreased brain water content, inhibiting an increase in ICP. These findings highlight the ongoing controversy among researchers regarding which drug therapy is preferred for treatment of TBI.[10–13] The lack of agreement is due, in part, to the complex pathophysiology of injury, involving multiple pathological processes: parenchymal inflammation, free radical production, increased intracellular calcium, lipid peroxidation, nitric oxide production, etc. Differential doses and timing of treatment, diverse models of trauma, animal type, and different measurement techniques are among other factors that also contribute to this ongoing controversy. As such, no clinical neuroprotective treatment is still available to date, and the search for the effective drug to prevent further brain damage is of great interest across the world. Based on our current findings, it is suggested that minocycline in combination with HTS may be an optimal therapy choice to mitigate the pathologies of head injury. Both drugs are safe, inexpensive, and have manageable side effects. As far as we are aware, this kind of combination has not been discussed to date. In contrast, our findings in mice indicate that using morphine and mannitol failed to provide adequate protection following trauma and could cause more severe injury. It is worth noting that the effectiveness of these drugs in term of their chemistry or physiologic effects was not evaluated nor compared during this study. Therefore, it may appear that although minocycline improved hemodynamic outcome, it may still be less effective pharmacologically. Future work is needed to investigate these effects and to correlate them with tissue optical and hemodynamic parameters. Furthermore, the results presented here provide the basis for further development of optical spectroscopy to quantify efficacy of neuroprotective therapies of TBI.

It should be pointed out that in typical DRS configurations, the use of a standard diffusion equation (SDE) for estimation of optical properties of tissue derived from diffuse reflectance measurement is used. The diffuse reflectance expression is calculated to semi-infinite geometry, where source and the detector are placed on the same surface. However, the use of the present model, where the emitter and detector are positioned perpendicularly, could yield false results. In addition, with a short SDS, 0.4 mm in our study, the use of diffusion theory is risky because it may not work in such conditions; SDE has been proven ineffective when SDS < 5 mm. To overcome these limitations of using the diffusion model, or rather using different approximations of light propagation in tissue (P3, δ-Eddington, δ-P1, etc.), we chose simply to first calculate the absorption coefficient using Beer's law in mode 2 (transmission mode) and then to estimate the reduced scattering coefficient throughout mode 1 (reflection geometry) using the linear relationship to the diffuse reflectance as demonstrated by several researchers.[30,42,100] The main advantage of this approach lies in its simplicity in terms of system configuration and optical properties extraction, less computation and in short time, and its potential application to study highly scattering thick tissue, such as the brain. In the near future, we plan to focus on the development of an appropriate mathematical expression for an orthogonal source–detector model. In spite of the above-mentioned advantages, one limitation of this approach could appear following adult human head monitoring; perpendicular positions of source and detector would bring a very large distance, i.e., ~10 cm. This would require the use of very sensitive detectors and high-power light sources (elevating costs) to increase the signal-to-noise ratio. In addition, measurement of wide spectrums in this case would be very difficult. Please note that these requirements are, on the contrary, unnecessary for monitoring infants' heads, due to the relative small SDS needed.

In summary, the optical setup utilized presently demonstrated its utility to study the efficacy of neuroprotective drug treatment early after focal TBI in a small animal model by simultaneously monitoring, noninvasively, brain hemodynamic parameters on a macroscopic level and assessing brain edema. We intend in future

studies to examine different doses and timing of drug administration with larger animal populations and to integrate behavioral tests with optical monitoring in order to further elaborate the results reported in this work. Additionally, the efficacy of minocycline, HTS, or the combination of the two should also be investigated in the future to determine the optimal drug treatment strategy. In general, neuroprotective drug treatment following TBI in the mice model is considered as an experimental platform mimicking the human response to TBI. In this context, the current method carries significant potential in clinical assessment of brain condition after neuroprotection administration.

References

1. M. R. Bullock and J. T. Povlishock, "Guidelines for the management of severe traumatic brain injury," *J. Neurotrauma* **24**, S1–S106 (2007).
2. M. Faul et al., "Traumatic Brain Injury in the United States: Emergency Department Visits, Hospitalizations and Deaths 2002–2006," Centers for Disease Control and Prevention National Center for Injury Prevention and Control, Atlanta, GA (2010).
3. J. H. Adams, D. I. Graham, and T. A. Gennarelli, "Head injury in man and experimental animals: neuropathology," *Acta Neurochir. Suppl. (Wien)* **32**, 15–30 (1983).
4. T. K. McIntosh et al., "Neuropathological sequelae of traumatic brain injury: relationship to neurochemical and biomechanical mechanisms," *Lab. Invest.* **74**(2), 315–342 (1996).
5. C. O. de Oliveira, N. Ikuta, and A. Regner, "Outcome biomarkers following severe traumatic brain injury," *Rev. Bras. Ter. Intensiva* **20**(4), 411–421 (2008).
6. B. F. Feyen et al., "Neuromonitoring in traumatic brain injury," *Minerva Anestesiol.* **78**(8), 949–958 (2012).
7. S. H. Friess, T. J. Kilbaugh, and J. W. Huh, "Advanced neuromonitoring and imaging in pediatric traumatic brain injury," *Crit. Care Res. Pract.* **2012**, 1–11 (2012).
8. J. G. Fujimoto and D. L. Farkas, *Biomedical Optical Imaging*, Oxford University Press, Oxford, New York (2009).
9. D. A. Boas, C. Pitris, and N. Ramanujam, *Handbook of Biomedical Optics*, CRC Press, Boca Raton, Florida (2011).
10. D. J. Loane and A. I. Faden, "Neuroprotection for traumatic brain injury: translational challenges and emerging therapeutic strategies," *Trends Pharmacol. Sci.* **31**(12), 596–604 (2010).
11. I. Maas, "Neuroprotective agents in traumatic brain injury," *Expert Opin. Investig. Drugs* **10**(4), 753–767 (2001).
12. A. Singh, P. Sharma, and S. Mishra, "Neuro-protection after traumatic brain injury: novel strategies," *J. Dent. Med. Sci.* **3**(6), 75–85 (2013).
13. J. Minnerup et al., "Neuroprotection for stroke: current status and future perspectives," *Int. Mol. Sci.* **13**, 11753–11772 (2012).
14. K. Kikuchi et al., "Clinical neuroprotective drugs for treatment and prevention of stroke," *Int. J. Mol. Sci.* **13**, 7739–7761 (2012).
15. Y. Xiong, A. Mahmood, and M. Chopp, "Emerging treatments for traumatic brain injury," *Expert Opin. Emerg. Drugs* **14**(1), 67–84 (2009).
16. S. V. Kabadi and A. I. Faden, "Neuroprotective strategies for traumatic brain injury: improving clinical translation," *Int. Mol. Sci.* **15**(1), 1216–1236 (2014).
17. S. Samantara et al., "Neuroprotective drugs in traumatic CNS injury," *Open Drug Discov. J.* **2**, 174–180 (2010).
18. D. S. Mortimer and J. Jancik, "Administering hypertonic saline to patients with severe traumatic brain injury," *J. Neurosci. Nurs.* **38**(3), 142–146 (2006).
19. H. Shawkat, M.-M. Westwood, and A. Mortimer, "Mannitol: a review of its clinical uses," *Anaesth. Crit. Care Pain* **12**(2), 82–85 (2012).
20. D. F. Kelly et al., "Propofol in the treatment of moderate and severe head injury: a randomized, prospective double-blinded pilot trial," *J. Neurosurg.* **90**(6), 1042–1052 (1999).
21. B. Cirak et al., "Melatonin as a free radical scavenger in experimental head trauma," *Pediatr. Neurosurg.* **31**(6), 298–301 (1999).
22. J. M. Plane et al., "Prospects for Minocycline neuroprotection," *Arch. Neurol.* **67**(12), 1442–1448 (2010).
23. M. A. Flierl et al., "Mouse closed head injury model induced by a weight-drop device," *Nat. Protoc.* **4**(9), 1328–1337 (2009).
24. O. Zohar et al., "Closed-head minimal traumatic brain injury produces long-term cognitive deficits in mice," *J. Neurosci.* **118**(4), 949–955 (2003).
25. S. Muehlschlegel et al., "Feasibility of NIRS in the neurointensive care unit: a pilot study in stroke using physiological oscillations," *Neurocrit. Care* **11**(2), 288–295 (2009).
26. M. Wolf, M. Ferrari, and V. Quaresima, "Progress of near-infrared spectroscopy and topography for brain and muscle clinical applications," *J. Biomed. Opt.* **12**(6), 062104 (2007).
27. H. Liu et al., "Near-infrared spectroscopy and imaging of tumor vascular oxygenation," *Methods Enzymol.* **386**, 349–378 (2004).
28. W. C. Lin et al., "Diffuse reflectance spectroscopy for *in vivo* pediatric brain tumor detection," *J. Biomed. Opt.* **15**(6), 061709 (2010).
29. J. Choi et al., "Noninvasive determination of the optical properties of adult brain: near-infrared spectroscopy approach," *J. Biomed. Opt.* **9**(1), 221–229 (2004).
30. G. Kumar and J. M. Schmitt, "Optimal probe geometry for near-infrared spectroscopy of biological tissue," *Appl. Opt.* **36**(10), 2286–2293 (1997).
31. A. Kim et al., "Fiber optic reflectance probe with multiple source-collector separations to increase the dynamic range of derived tissue optical absorption and scattering coefficients," *Opt. Express* **18**(6), 5580–5594 (2010).
32. J. T. E. Richardson, *Clinical and Neuropsychological Aspects of Closed Head Injury*, 2nd ed., Psychology Press, Philadelphia (2002).
33. R. L. Rodnitzky and M. Meier, "Neurobehavioral consequences of closed head injury," *Arch. Neurol.* **39**(10), 675–676 (1982).
34. D. Abookasis, A. Shochat, and M. S. Mathews, "Monitoring hemodynamic and morphologic responses to closed head injury in a mouse model using orthogonal diffuse near-infrared light reflectance spectroscopy," *J. Biomed. Opt.* **18**(4), 045003 (2013).
35. D. Abookasis, B. Volkov, and M. S. Mathews, "Closed head injury-induced changes in brain pathophysiology assessed with near-infrared structured illumination in a mouse model," *J. Biomed. Opt.* **18**(11), 116007 (2013).
36. S. Fantini, M. A. Franceschini, and E. Gratton, "Effective source term in the diffusion equation for photon transport in turbid media," *Appl. Opt.* **36**(1), 156–163 (1997).
37. H. Z. Yeganeh et al., "Broadband continuous-wave technique to measure baseline values and changes in the tissue chromophore concentrations," *Biomed. Opt. Express* **3**(11), 2761–2770 (2012).
38. R. Watté et al., "Metamodeling approach for efficient estimation of optical properties of turbid media from spatially resolved diffuse reflectance measurements," *Opt. Express* **21**(26), 32630–32642 (2013).
39. A. Kim et al., "A fiber optic reflectance probe with multiple source-collector separations to increase the dynamic range of derived tissue optical absorption and scattering coefficients," *Opt. Express* **18**(6), 5580–5594 (2010).
40. C. Lau et al., "Re-evaluation of model-based light-scattering spectroscopy for tissue spectroscopy," *J. Biomed. Opt.* **14**(2), 024031 (2009).
41. G. Zonios and A. Dimou, "Light scattering spectroscopy of human skin *in vivo*," *Opt. Express* **17**(3), 1256–1267 (2009).
42. M. Johns et al., "Determination of reduced scattering coefficient of biological tissue from a needle-like probe," *Opt. Express* **13**(13), 4828–4842 (2005).
43. G. Strangman, M. A. Franceschini, and D. A. Boas, "Factors affecting the accuracy of near-infrared spectroscopy concentration calculations for focal changes in oxygenation parameters," *Neuroimage* **18**(4), 865–879 (2003).
44. D. T. Delpy et al., "Estimation of optical pathlength through tissue from direct time of flight measurement," *Phys. Med. Biol.* **33**(12), 1433–1442 (1988).
45. A. Li et al., "Reconstructing chromosphere concentration images directly by continuous-wave diffuse optical tomography," *Opt. Lett.* **29**(3), 256–258 (2004).
46. A. Bhardwaj and J. A. Ulatowski, "Hypertonic saline solutions in brain injury," *Curr. Opin. Crit. Care* **10**(2), 126–131 (2004).
47. S. Berger and R. Hartl, "Traumatic brain injury and use of hypertonic solutions," *Transfus. Altern. Transfus. Med.* **6**(4), 59–68 (2005).
48. D. S. Mortimer and J. Jancik, "Administering hypertonic saline to patients with severe traumatic brain injury," *J. Neurosci. Nurs.* **38**(3), 142–154 (2006).
49. C. Wood and B. A. Boucher, "Management of acute traumatic brain injury," 2012, https://www.accp.com/docs/bookstore/psap/p7b10sample03.pdf (3 January 2015).

50. D. S. DeWitt et al., "Reduced cerebral blood flow, oxygen delivery, and electroencephalographic activity after traumatic brain injury and mild hemorrhage in cats," *J. Neurosurg.* **76**(5), 812–821 (1992).
51. L. M. Foley et al., "MRI assessment of cerebral blood flow after experimental traumatic brain injury combined with hemorrhagic shock in mice," *J. Cereb. Blood Flow Metab.* **33**, 129–136 (2012).
52. M. Zaaroor et al., "Course of cerebral blood flow and metabolism following severe brain injury. Correlation with neurological function and outcome," *Indian J. Neurotrauma* **4**(1), 25–29 (2007).
53. P. Bouzat et al., "Beyond intracranial pressure: optimization of cerebral blood flow, oxygen, and substrate delivery after traumatic brain injury," *Ann. Intensive Care* **3**(1), 1–9 (2013).
54. C. Zhou et al., "Diffuse optical monitoring of hemodynamic changes in piglet brain with closed head injury," *J. Biomed. Opt.* **14**(3), 034015 (2009).
55. Y. Jia et al., "*In vivo* optical imaging of revascularization after brain trauma in mice," *Microvasc. Res.* **81**(1), 73–80 (2011).
56. H. White, D. Cook, and B. Venkatesh, "The use of hypertonic saline for treating intracranial hypertension after traumatic brain injury," *Anesth. Analg.* **102**(6), 1836–1846 (2006).
57. M. M. Mortazavi et al., "Hypertonic saline for treating raised intracranial pressure: literature review with meta-analysis," *J. Neurosurg.* **116**(1), 210–221 (2012).
58. S. E. Robinson et al., "The effects of morphine and traumatic brain injury on central cholinergic neurons," *Brain Res.* **503**(1), 32–37 (1989).
59. O. Zohar et al., "Morphine protects for head trauma induced cognitive deficits in mice," *Neurosci. Lett.* **394**(3), 239–242 (2006).
60. S. E. Hocker, J. Fogelson, and A. A. Rabinstein, "Refractory intracranial hypertension due to fentanyl administration following closed head injury," *Front. Neurol.* **4**(3), 1–3 (2013).
61. T. L. Holbrook et al., "Morphine use after combat injury in Iraq and post-traumatic stress disorder," *N. Engl. J. Med.* **362**(2), 110–117 (2010).
62. M. de Nadal et al., "Cerebral hemodynamic effects of morphine and fentanyl in patients with severe head injury: absence of correlation to cerebral autoregulation," *Anesthesiology* **92**(1), 11–19 (2000).
63. K. K. Lauer, L. A. Connolly, and W. T. Schmeling, "Opioid sedation does not alter intracranial pressure in head injured patients," *J. Can. Anaesth.* **44**(9), 929–933 (1997).
64. L. D. Mishra, N. Rajkumar, and S. M. Hancock, "Current controversies in neuroanaesthesia, head injury management and neuro critical care," *Crit. Care Pain* **6**(2), 79–82 (2006).
65. K.-C. Lin et al., "The early response of mannitol infusion in traumatic brain injury," *Acta Neurol. Taiwan* **17**(1), 26–32 (2008).
66. M. N. Diringer et al., "Effect of mannitol on cerebral blood volume in patients with head injury," *Neurosurgery* **70**(5), 1215–1219 (2012).
67. A. Wakai et al., "Mannitol for acute traumatic brain injury," *Cochrane Database Syst. Rev.* **24**(1), 1–14, (2007).
68. A. A. Wani et al., "Controversy in use of mannitol in head injury," *J. Indian Neurotrauma* **5**(1), 11–13 (2008).
69. T. Dziedzic et al., "Is mannitol safe for patients with intracerebral hemorrhages? Renal considerations," *Clin. Neurol. Neurosurg.* **105**, 87–90 (2003).
70. J. Xie et al., "Minimally invasive assessment of the effect of mannitol and hypertonic saline therapy on traumatic brain edema using measurements of reduced scattering coefficient (μ_s')," *Appl. Opt.* **49**(28), 5407–5414 (2010).
71. J. P. Muizelaar, H. A. Lutz, and D. P. Becker, "Effect of mannitol on ICP and CBF and correlation with pressure autoregulation in severely head-injured patients," *Neurosurgery* **61**(4), 700–706 (1984).
72. C. Mesenge et al., "Protective effect of melatonin in a model of traumatic brain injury in mice," *J. Pineal Res.* **25**(1), 41–46 (1998).
73. S. M. Beni et al., "Melatonin-induced neuroprotection after closed head injury is associated with increased brain antioxidants and attenuated late-phase activation of NF-kappaB and AP-1," *J. Fed. Am. Soc. Exp. Biol.* **18**(1), 149–151 (2004).
74. S. Samantaray et al., "Therapeutic potential of melatonin in traumatic central nervous system injury," *J. Pineal Res.* **47**(2), 134–142 (2009).
75. R. J. Reiter and D.-X. Tan, "Melatonin: a novel protective agent against oxidative injury of the ischemic/reperfused heart," *Cardiovasc. Res.* **58**(1), 10–19 (2003).
76. O. Ates et al., "Effect of pinealectomy and melatonin replacement on morphological and biochemical recovery after traumatic brain injury," *J. Int. Dev. Neurosci.* **24**(6), 357–363 (2006).
77. D. Ozdemir et al., "Effect of melatonin on brain oxidative damage induced by traumatic brain injury in immature rats," *Physiol. Res.* **54**(6), 631–637 (2005).
78. A. S. Sarrafzadeh et al., "Neuroprotective effect of melatonin on cortical impact injury in the rat," *Acta Neurochir.* **142**(11), 1293–1299 (2000).
79. E. Esposito and S. Cuzzocrea, "Antiinflammatory activity of melatonin in central nervous system," *Curr. Neuropharmacol.* **8**(3), 228–242 (2010).
80. A. Bayir et al., "The effects of mannitol and melatonin on MRI findings in an animal model of traumatic brain edema," *Acta Neurol. Belg.* **108**(4), 149–154 (2008).
81. F. Dehghan et al., "Effect of melatonin on intracranial pressure and brain edema following traumatic brain injury: role of oxidative stresses," *Arch. Med. Res.* **44**(4), 251–258 (2013).
82. A. Görgülü et al., "Effect of melatonin on cerebral edema in rats," *Neurosurgery* **49**(6), 1434–1441 (2001).
83. E. J. Lee et al., "Melatonin attenuates gray and white matter damage in a mouse model of transient focal cerebral ischemia," *J. Pineal Res.* **38**(1), 42–52 (2005).
84. S. Samantaray et al., "Melatonin attenuates calpain upregulation, axonal damage and neuronal death in spinal cord injury in rats," *J. Pineal Res.* **44**(4), 348–357 (2008).
85. M. L. Kelso et al., "Melatonin and minocycline for combinatorial therapy to improve functional and histopathological deficits following traumatic brain injury," *Neurosci. Lett.* **488**(1), 60–64 (2011).
86. J. Wu et al., "Minocycline reduces intracerebral hemorrhage-induced brain injury," *Neurol. Res.* **31**(2), 183–188 (2009).
87. M. Tsuji et al., "Minocycline worsens hypoxic-ischemic brain injury in a neonatal mouse model," *Exp. Neurol.* **189**(1), 58–65 (2004).
88. D. Blum et al., "Clinical potential of minocycline for neurodegenerative disorders," *Neurobiol. Dis.* **17**(3), 359–366 (2004).
89. D. Zemke and A. Majid, "The potential of minocycline for neuroprotection in human neurologic disease," *Clin. Neuropharmacol.* **27**(6), 293–298 (2004).
90. M. Chen et al., "Minocycline inhibits caspase-1 and caspase-3 expression and delays mortality in a transgenic mouse model of Huntington disease," *Nat. Med.* **6**(7), 797–801 (2000).
91. J. M. Plane et al., "Prospects for minocycline neuroprotection," *Arch. Neurol.* **67**(12), 1442–1448 (2010).
92. F. Zhao et al., "Minocycline-induced attenuation of iron overload and brain injury after experimental intracerebral hemorrhage," *Stroke* **42**(12), 3587–3593 (2011).
93. N. Bye et al., "Transient neuroprotection by minocycline following traumatic brain injury is associated with attenuated microglial activation but no changes in cell apoptosis or neutrophil infiltration," *Exp. Neurol.* **204**(1), 220–233 (2007).
94. S. Homsi et al., "Minocycline effects on cerebral edema: relations with inflammatory and oxidative stress markers following traumatic brain injury in mice," *Brain Res.* **1291**, 122–132 (2009).
95. J. K. Wasserman and L. C. Schlichter, "Minocycline protects the blood–brain barrier and reduces edema following intracerebral hemorrhage in the rat," *Exp. Neurol.* **207**(2), 227–237 (2007).
96. P. I. Thompson et al., "Respiratory depression following morphine and morphine-6-glucuronide in normal subjects," *J. Br. Clin. Pharmacol.* **40**(2), 145–152 (1995).
97. J. L. Hinkle and K. H. Cheever, *Brunner & Suddarth's Textbook of Medical-Surgical Nursing*, 13th ed., Lippincott Williams & Wilkins, Philadelphia (2014).
98. L. F. Marshall et al., "Mannitol dose requirements in brain-injured patients," *J. Neurosurg.* **48**(2), 169–172 (1978).
99. D. Yildizdas et al., "Hypertonic saline treatment in children with cerebral edema," *Indian Pediatr.* **43**(9), 771–779 (2006).
100. S. C. Kanick et al., "Scattering phase function spectrum makes reflectance spectrum measured from Intralipid phantoms and tissue sensitive to the device detection geometry," *Biomed. Opt. Express* **3**(5), 1086–1100 (2012).

Biographies of the authors are not available.